JOC Article

Computational DFT Investigation of Vicinal Amide Group Anchimeric Assistance in Ether Cleavage

Matteo Calvaresi,[†] Samuele Rinaldi,*[,‡] Antonio Arcelli,[†] and Marco Garavelli*[,†]

Dipartimento di Chimica "G. Ciamician", Università di Bologna, Via Selmi 2, 40126 Bologna, Italy, and Dipartimento di Scienze e Tecnologie Chimiche, Università Politecnica delle Marche, Via Brecce Bianche 1-60131 Ancona, Italy

marco.garavelli@unibo.it; s.rinaldi@univpm.it

Received June 27, 2007

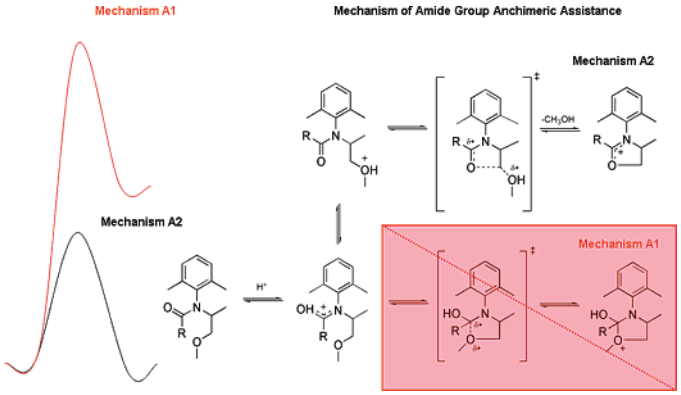

Density functional theory (DFT) computations in solvent have been used to investigate the mechanism of anchimeric assistance (by a vicinal amide group) in the acid-induced ether cleavage. The calculations were carried out at the B3LYP/6-31G* level of theory via full geometry optimizations within the IEF-PCM continuum solvent model. Two different mechanisms have been investigated here that were previously hypothesized for the rate-determining step of this process: the first (mechanism **A1**) involves a protonated amide and an ethereal oxygen as the nucleophile, while the second (mechanism **A2**) involves protonation of the ethereal oxygen followed by a nucleophilic attack of the amide. Computations clearly show that the second (involving protonation of the less basic site) is the most favorite route and leads to the formation of an oxazolidinic intermediate that triggers ether hydrolysis. Results are produced that are in excellent agreement with the experiments, and a rationale for them is provided, which represents a general interpretative basis for similar anchimerically assisted processes, such as the ones characterizing the glycosidic activity of two very important classes of enzymes: β-hexosaminidases and O-GlcNAcases.

Introduction

In the last 50 years, the intramolecular participation of vicinal groups has been extensively studied because anchimeric assistance is a major topic in organic chemistry.[1−8] From the pioneering studies by Winstein and Buckles[9] in 1942, a lot of work has been focused on systems involving "intramolecular catalysis" such as nucleophilic catalysis in ester hydrolysis.[7,10] However, there are very few examples in the literature of application of neighboring amide group participation[11] in organic

[†] Università di Bologna.
[‡] Università Politecnica delle Marche.

(1) Kirby, A. J.; Williams, N. H. *J. Chem. Soc., Chem. Commun.* **1991**, 1463.
(2) Kirby, A. J.; Williams, N. H. *J. Chem. Soc., Chem. Commun.* **1991**, 1464.
(3) Bruice, T. C.; Pandit, U. K. *J. Am. Chem. Soc.* **1960**, *82*, 5858−5865.
(4) Menger, F. M. *Acc. Chem. Res.* **1985**, *18*, 128−134.
(5) Page, M. I.; Jencks, W. P. *Proc. Natl. Acad. Sci. U.S.A.* **1971**, *68*, 1678−1683.
(6) Houk, K. N.; Tucker, J. A. *Acc. Che. Res.* **1990**, *23*, 107−113.
(7) Lighstone, F. C.; Bruice, T. C. *J. Am. Chem. Soc.* **1996**, *118*, 2595−2605.
(8) Lighstone, F. C.; Bruice, T. C. *Acc. Chem. Res.* **1999**, *32*, 127−136.
(9) Winstein, S.; Buckles, R. E. *J. Am. Chem. Soc.* **1942**, *64*, 2780−2786.
(10) Andres, G. O.; Pierini, A. B.; de Rossi, R. H. *J. Org. Chem.* **2006**, *71*, 7650−7656.

10.1021/jo701394z CCC: $40.75
Published on Web 02/21/2008

SCHEME 1

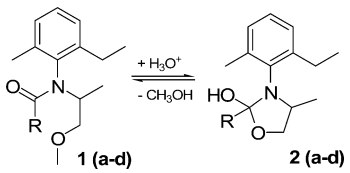

TABLE 1. Experimental Activation Free Energy Barriers for the Acid Hydrolysis of Substrates 1a−d (The Kinetic Data, Taken from Ref 23, are Observed at 50° and 1 atm)

substrate **1**	$\Delta G^{\ddagger}$
(**1a**) R = CH_3	25.8 ± 1.5
(**1b**) R = C_2H_5	24.9 ± 0.7
(**1c**) R = $CH(CH_3)_2$	24.1 ± 0.5
(**1d**) R = $C(CH_3)_3$	22.4 ± 0.7

synthesis. This topic is very significant in biochemistry because the catalytic activity of important enzymes such as the glycosidase β-hexosaminidases[12,13] and O-GlcNAcases[14−16] has been recently shown to involve anchimeric assistance from the acetamido group of the substrate that promotes glycosidic bond breaking.

In previous papers, we reported the first example of acid-induced ether cleavage anchimerically assisted by a vicinal amide group.[17−23] The amide group catalyzes the acid hydrolysis of a vicinal methyl ether linkage in relatively mild conditions. The rate of enhancement caused by the assistance of the vicinal group was kinetically measured to be at least 1.7×10^3-fold higher than that of a reference compound without the amide function.[17] In fact, the neighboring amide group triggers the formation of an oxazolidinic intermediate whose hydrolysis is easier than direct cleavage of the methyl group. Additionally, in our studies, we also observed that the hydrolytic process rate is strongly affected by the bulkiness of the group (R) of the substrate **1** (see Scheme 1). The kinetic studies performed on substrates **1a−d** (see Table 1) showed that the increased bulkiness of R causes a considerable accelerating effect on the anchimerically assisted hydrolytic process of the ether bond: at 57.8 °C, the hydrolysis rate of **1d** (R = *t*Bu) is more than 100-fold higher than that of the substrate **1a** (R = Me).[23]

Two reaction paths have been suggested for the conversion of **1** to **2** (Scheme 2). In the first route (**A1** mechanism), the ethereal oxygen participates as a nucleophile and attacks the protonated amide group, while the second pathway (**A2** mechanism[24]) involves protonation of the ethereal oxygen followed by the nucleophilic attack of the amide group. In both cases, the amide group participates in the formation of a cyclic pentatomic intermediate (postulated to be cationic), which is the substrate for the following nucleophilic attack by a water molecule to give the final oxazolidine derivative **2**. It is apparent that the reactive process is controlled by the balance between different and opposite effects, whose final outcome will be to select the most favorite route: while **A1** implies the protonation of the most favorite site (i.e., the most basic amidic carbonyl) followed by the attack of a worse nucleophile (i.e., the ether), **A2** involves the protonation of the ethereal oxygen (that is disadvantageous from a thermodynamic point of view), but then the attack of a stronger nucleophile (i.e., the amidic carbonyl) occurs.

In order to shed light upon the anchimeric assistance-based mechanism followed by these reactions, and in particular to explain the surprisingly high reaction rate shown by the substrate **1d** with respect to **1a**, a density functional theory (DFT) computational investigation has been performed on the acid-induced ether cleavage of both compounds in water. Besides supplying a nice rationale for the observations, which is in agreement with the recorded data, the investigated system is suggested to represent a general biomimetic model for the anchimerically assisted glycosidase activity of β-hexosaminidases and O-GlcNAcases, thus providing a reference reactivity scheme for the catalytic activity of this important class of enzymes.

Computational Methods

A preliminary conformational analysis was performed to determine the best conformation of the reactant and its protonated form in water. For this purpose, the program Macromodel 5.5[25] was used with the MM2[26] parameters for reactants and the semiempirical PM3[27] for the protonated species. Implicit solvation models were used to simulate the presence of solvent. It was carried out with a Monte Carlo search with six torsional angles and 1000 steps for torsion. All the local minima within 50 kJ mol^{-1} with respect to

(11) Cohen, T.; Lipowitz, J. *J. Am. Chem. Soc.* **1964**, *86*, 5611−5616.
(12) Knapp, S.; Vocadlo, D. J.; Gao, Z. N.; Kirk, B.; Lou, J. P.; Withers, S. G. *J. Am. Chem. Soc.* **1996**, *118*, 6804−6805.
(13) Mark, B. L.; Vocadlo, D. J.; Knapp, S.; Triggs-Raine, B. L.; Withers,S. G.; James, M. N. *J. Biol. Chem.* **2001**, *276*, 10330−10337.
(14) Macauley, M. S.; Whitworth, G. E.; Debowski, A. W.; Chin, D.; Vocadlo, D. J. *J. Biol. Chem.* **2005**, *280*, 25313−25322.
(15) Cetinbas, N.; Macauley, M. S.; Stubbs, K. A.; Drapala, R.; Vocadlo, D. J. *Biochemistry* **2006**, *45*, 3835−3844.
(16) Dennis, R. J.; Taylor, E. J.; Macauley, M. S.; Stubbs, K. A.; Turkenburg, J. P.; Hart, S. J.; Black, G. N.; Vocadlo, D. J.; Davies G. J. *Nat. Struct. Biol. 13*, 365−371.
(17) Arcelli, A.; Porzi, G.; Sandri, S. *Tetrahedron* **1995**, *51*, 9729−9736.
(18) Arcelli, A.; Papa, M.; Porzi, G.; Sandri, S. *Tetrahedron* **1997**, *53*, 10513−10516.
(19) Arcelli, A.; Porzi, G.; Rinaldi, S.; Sandri, S. *J. Chem. Soc., Perkin Trans. 2* **2001**, 296−301.
(20) Arcelli, A.; Cecchi, R.; Porzi, G.; Rinaldi, S.; Sandri, S. *Tetrahedron* **2001**, *57*, 4039−4043.
(21) Arcelli, A.; Cecchi, R.; Porzi, G.; Rinaldi, S.; Sandri, S. *Tetrahedron* **2001**, *57*, 6843−6846.
(22) Arcelli, A.; Paradisi, F.; Porzi, G.; Rinaldi, S.; Sandri, S. *J. Chem. Res. (S)* **2002**, *199*, 501.
(23) Arcelli, A.; Porzi, G.; Rinaldi, S.; Sandri, S. *J. Phys. Org. Chem.* **2004**, *17*, 289−293.
(24) Strictly speaking, **A2** means bimolecular in contrast with the unimolecularity of the cyclization step. However, here we have retained this term in the sense that this is a bimolecular nucleophilic substitution in which the leaving group first acquires a proton. More correctly, this process should be termed an **A2** ***like mechanism***.
(25) Mohamadi, F.; Richards, N. G. J.; Guida, W. C.; Liskamp, R.; Lipton, M.; Caufield, C.; Chang, G.; Henrickson, T.; Still, W. C. *J. Comput. Chem.* **1990**, *11*, 440−467.
(26) Allinger, N. L. *J. Am. Chem. Soc.* **1977**, *99*, 8127−8134.
(27) Stewart, J. J. P. *J. Comput. Chem.* **1989**, *209*, 221−264.
(28) Frisch, M. J.; Trucks, G. W.; Schlegel, H. B.; Scuseria, G. E.; Robb, M. A.; Cheeseman, J. R.; Montgomery, J. A., Jr.; Vreven, T.; Kudin, K. N.; Burant, J. C.; Millam, J. M.; Iyengar, S. S.; Tomasi, J.; Barone, V.; Mennucci, B.; Cossi, M.; Scalmani, G.; Rega, N.; Petersson, G. A.; Nakatsuji, H.; Hada, M.; Ehara, M.; Toyota, K.; Fukuda, R.; Hasegawa, J.; Ishida, M.; Nakajima, T.; Honda, Y.; Kitao, O.; Nakai, H.; Klene, M.; Li, X.; Knox, J. E.; Hratchian, H. P.; Cross, J. B.; Bakken, V.; Adamo, C.; Jaramillo, J.; Gomperts, R.; Stratmann, R. E.; Yazyev, O.; Austin, A. J.; Cammi, R.; Pomelli, C.; Ochterski, J. W.; Ayala, P. Y.; Morokuma, K.; Voth, G. A.; Salvador, P.; Dannenberg, J. J.; Zakrzewski, V. G.; Dapprich, S.; Daniels, A. D.; Strain, M. C.; Farkas, O.; Malick, D. K.; Rabuck, A. D.; Raghavachari, K.; Foresman, J. B.; Ortiz, J. V.; Cui, Q.; Baboul, A. G.; Clifford, S.; Cioslowski, J.; Stefanov, B. B.; Liu, G.; Liashenko, A.; Piskorz, P.; Komaromi, I.; Martin, R. L.; Fox, D. J.; Keith, T.; Al-Laham, M. A.; Peng, C. Y.; Nanayakkara, A.; Challacombe, M.; Gill, P. M. W.; Johnson, B.; Chen, W.; Wong, M. W.; Gonzalez, C.; Pople, J. A. *Gaussian 03*, revision C.02; Gaussian, Inc.: Wallingford, CT, 2004.

the absolute minimum were retained for further quantum mechanical (QM) calculations. All QM calculations were performed with the Gaussian 03 suite of programs.[28] All the molecular geometries were optimized at the DFT level using Becke's three-parameters exchange functional in conjunction with the Lee−Yang−Parr correlation functional (B3LYP).[29] For all the atoms, the 6-31G* basis set was used. Larger basis sets (e.g., containing diffuse functions to better describe the heteroatom lone pairs) are usually required to achieve quantitative results for these kinds of reactions. However, giving the excellent agreement with the experimental results obtained with this basis set and since the energies computed for the two alternative routes (**A1** and **A2**) are very different, we think that our conclusions are adequately supported using this level of theory. To take into account bulk solvent effects, full geometry optimizations within a continuum solvent model (with water as solvent) were carried out via the self-consistent reaction field (SCRF) approach, using the polarizable continuum model (IEF-PCM) method.[30−32]

Calculations of the harmonic vibrational frequencies were carried out to determine the nature of each optimized critical point. For the transition states, inspection of the negative frequency was sufficient to specify the corresponding reaction path. Unscaled vibrational frequencies were used to calculate zero-point energy (ZPE) corrections to the total energy. The Gibbs free energies were then calculated employing the usual approximations of statistical thermodynamics (ideal gas, harmonic oscillator, and rigid rotor) at the temperature of 323.15 K and the pressure of 1.00 atm (which are the experimental conditions used for recording the activation barriers reported in Table 1[23]). Gibbs free energy values are always used for discussing the energetics. Partial charges were computed following the standard ESP fitting procedure: the used quantum electrostatic potential was sampled by the Merz−Singh−Kollman (MK) scheme.[33,34]

The system used in the calculation differs from that of the kinetic study only for one of the phenyl ring substituents: while the experimental system has a methyl and an ethyl substituent at positions 2 and 6 of the phenyl ring, only methyl substituents were used for the model system. Experiments show that this change does not affect the kinetics of the process,[19,22] while computations (and the conformational analysis) are made more efficient.

Results and Discussion

Since kinetic data[17−19,22,23] reveal that the reactions consist of a rapid equilibrium between protonated and unprotonated reactant, followed by the rate-determining step of acid-induced ether hydrolysis[19] (i.e., the postulated cyclization to the oxonium cation), only the protonation equilibrium and the cyclization were investigated here for the two proposed (**A1** and **A2**) mechanisms.

(a) Protonation Equilibrium. The first step of our study is to check the stability of the two possible different protomers derived from protonation of the amidic carbonyl (**ProtA1**) or the ethereal oxygen (**ProtA2**), respectively. These protomers have been assumed to be in a rapid equilibrium by means of direct proton exchange or exchange with solvent molecules.

There are a lot of ways to calculate computationally the acidity/basicity of a molecule, from the simplest methods in which solvation effects are taken into account using dielectric continuum models (these models fail to include short-range effects such as hydrogen bonding that can be important in determining accurate pK_a values[35]) to the possibility of including explicitly one or more water molecules of the first solvation shell[36,37] (anyway the transferred proton is not necessarily associated with the first solvation shell in aqueous solution) until the most efficient QM/MM simulations that account for bulk solvent effects.[38] Here, we need only to have a first rough estimate of the basicity of the two sites (i.e., we need only to know the relative stability of the two protomers and, consequently, the starting point of the cyclization reaction that is the bottleneck of the whole process). This was done using a very simple model based on a "naked proton" and implicit solvent. Obviously, this procedure implies several errors/approximations (vide infra).

If we take *N*,*N*-dimethylacetamide as a model for the carbonyl amide (experimental pK_a of the protonated species $= -0.28$[39]) and dimethyl ether as a model for the ether (experimental pK_a of the protonated species $= -3.8$[40]), it is clear that the primary site of protonation is the amidic carbonyl. Our computations confirm this result, showing that protonation of the amidic carbonyl is exergonic both in the presence (13.5 and 14.2 kcal mol^{-1} for R = Me and R = *t*Bu, respectively) and in the absence (7.7 and 10.2 kcal mol^{-1} for R = Me and R = *t*Bu, respectively) of an intramolecular hydrogen bond with the ethereal oxygen, while protonation of the ether is always endergonic (6.6 and 5.6 kcal mol^{-1} for R = Me and R = *t*Bu, respectively) (see Figure S1 in the Supporting Information for optimized structures and energies of the protomers). However, the computed energy differences for the protonation of the amidic carbonyl *without* an intramolecular hydrogen bond (the proper reference to compare with *N*,*N*-dimethylacetamide) versus the ethereal oxygen are 14.3 and 15.8 kcal mol^{-1} (corresponding to 9.7 and 10.7 pK_a units) for R = Me and R = *t*Bu, respectively, while the experimental value referring to *N*,*N*-dimethylacetamide and dimethyl ether amounts to only 3.5 pK_a units (or 5.2 kcal mol^{-1}).

It is apparent that our results poorly reproduce experimental data (they can reproduce just qualitatively the relative basicity of the two sites). This difference is mainly due to the difficulty of DFT methods (and the B3LYP functional in particular) to model protonated ethers (such as **ProtA2**) as shown by Carlier et al.[41] and by Truhlar and Zhao.[42] It is also due in part to the basis set used (lacking diffuse functions) and the lack of explicit water molecules (i.e., naked proton model; indeed, using a B3LYP functional with two explicit waters, the computed energy difference is lowered to 11 kcal mol^{-1}).[43] In other words, this simplified model/level of theory is not suitable for a reliable pK_a estimate, as expected. However, our aim is not to reproduce the pK_a of the molecule but only to confirm the protonation of the amide as the right starting point for the cyclization reaction. Additionally, we are persuaded that the errors involved do not

(29) Becke, A. D. *J. Chem. Phys.* **1993**, *98*, 5648−5652.
(30) Cancès, M. T.; Mennucci, B.; Tomasi, J. *J. Chem. Phys.* **1997**, *107*, 3032−3041.
(31) Cossi, M.; Barone, V.; Mennucci, B.; Tomasi, J. *Chem. Phys. Lett.* **1998**, *286*, 253−260.
(32) Mennucci, B.; Tomasi, J. *J. Chem. Phys.* **1997**, *106*, 5151−5158.
(33) Singh, U. C.; Kollman, P. A. *J. Comput. Chem.* **1983**, *4*, 129−145.
(34) Besler, B. H.; Merz, K. M.; Kollman, P. A. *J. Comput. Chem.* **1990**, *11*, 431−439.
(35) Chipman, D. M. *J. Phys. Chem. A* **2002**, *106*, 7413−7422.
(36) Nguyen, M. T.; Raspoet, G.; Vanquickenborne, L. G. *J. Am. Chem. Soc.* **1997**, *119*, 2552−2562.
(37) Pliego, J. R., Jr.; Riveros, J. M. *J. Phys. Chem. A* **2001**, *105*, 7241−7247.
(38) Zahn, D.; Schmidt, K. F.; Kast, S. M.; Brickmann, J. *J. Phys. Chem. A* **2002**, *106*, 7807−7812.
(39) Grant, H. M.; Mctigue, P.; Ward, D. G. *Aust. J. Chem.* **1983**, *36*, 2211−2218.
(40) Arnett, E. M.; Wu, C. Y. *J. Am. Chem. Soc.* **1962**, *84*, 1680−1684.
(41) Carlier, P. R.; Deora, N.; Crawford, T. D. *J. Org. Chem.* **2006**, *71*, 1592−1597.
(42) Zhao, Y.; Truhlar, D. G. *J. Org. Chem.* **2007**, *72*, 295−298.
(43) Hori, K.; Ikenaga, Y.; Arata, K.; Takahashi, T.; Kasai, K.; Noguchi, Y.; Sumimoto, M.; Yamamoto, H. *Tetrahedron* **2007**, *63*, 1264−1269.

SCHEME 2

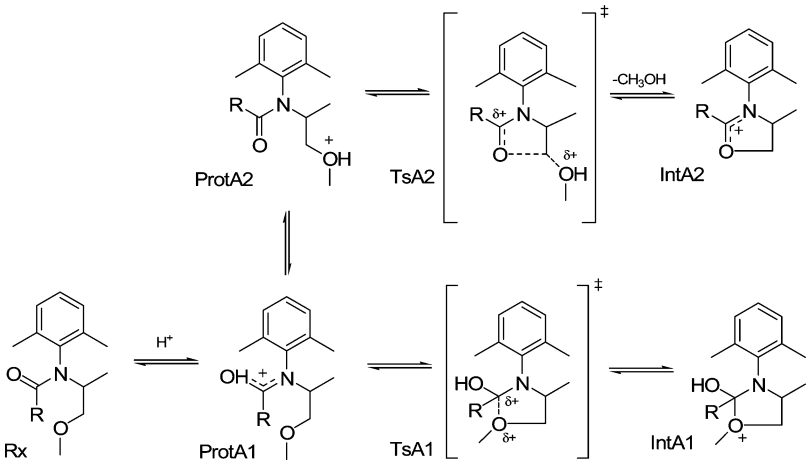

influence the size of the overall calculated barriers (that are the quantities that must be compared to the experimental kinetic data) because they do mainly affect the relative position of the intermediate state (the protonated ether **ProtA2**; see Scheme 2) and not the one of the rate-determining transition state, with respect to the starting and stable protomer (**ProtA1**; see also the Supporting Information). Finally, as the errors/approximations implicated in this procedure are always the same regardless the substituent (R = Me or *t*Bu), a comparison of the results computed for the two substituted systems (vide infra) should lead to quantitatively reliable conclusions. The good agreement with the experimental barriers (see the discussion below) does support this view.

The two systems (R = Me and R = *t*Bu) show a different stability for the protonation of the amidic carbonyl (the molecule with the *t*Bu substituent is 0.7 kcal mol^{-1} more stable than that with R = Me). This can be easily explained on the basis of the different electronic effects of the two amidic carbonyl substituents (R). In fact, it is well-known that the higher the electron-donating effect of the substituent, the higher the basicity of the carbonyl group, owing to a greater stabilization (by resonance/inductive effects) of the positive charge caused by the protonation. It is apparent that *t*Bu (which is a better electron-donating group than methyl) does better stabilize the protonated carbonyl leading to a slightly more stable conformer.

(b) A1 and A2 Mechanisms. As the starting (i.e., more stable) point of the process is the protonated carbonyl, we first investigated the **A1** route. Surprisingly, despite several attempts, it was impossible to locate the cationic oxonium intermediate (**IntA1**) and the corresponding transition state (**TsA1**) that links this point to the starting protonated reactant (**ProtA1**). In an attempt to stabilize the **IntA1** product, we also added an explicit water molecule, yet this try was unsuccessful. These preliminary results raised some doubts about the effectiveness of this path, especially considering the lack of stability of the postulated intermediate. Consequently, in light of these results, the alternative mechanism **A1′** was suggested (see Scheme 3), in which a water molecule does directly participate in the process by carrying out a concerted attack on the methyl ether during the cyclization process.

This path directly leads to the neutral cyclization product **IntA1′** via a single concerted transition state (**TsA1′**), without involving (i.e., bypassing) the cationic intermediate **IntA1**.

We were able to locate the transition state (**TsA1′**) for this path for both the Me and *t*Bu substituents, even if it turns out

SCHEME 3

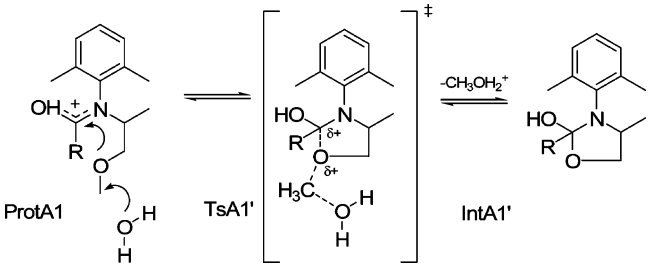

to be at much higher energy then the experimentally recorded values[23] (see Table 1 and Figure 1).

In fact, a barrier of 54.8 and 53.0 kcal mol^{-1} was found for R = Me and for R = *t*Bu, respectively, while the experimentally recorded one[23] is 25.8 ± 1.5 (R = Me) and 22.4 ± 0.7 (R = *t*Bu). At **TsA1′** (see Figure 2), the bond between the carbonylic carbon and the ethereal oxygen is almost completely formed (for R = Me and R = *t*Bu the lengths are 1.47 and 1.50 Å, respectively), while the leaving methyl group appears between the ethereal and water oxygens (1.93 and 2.01 Å for R = Me and 1.94 and 2.00 Å for R = *t*Bu). Additionally, it appears that the cyclization product **IntA1′** is endergonic (40.3 and 37.0 kcal mol^{-1} vs **ProtA1** for R = Me and R = *t*Bu, respectively), so that the **A1**/**A1′** routes seem to be very much unlikely in any case.

The **A2** mechanism was then explored. In order to compare energetically this route with the previous one, one explicit water molecule was also introduced (so doing, the reacting system is exactly the same for both the **A1′** and **A2** routes), even if this water is not necessary for locating the critical points of this second path. Inspection of the imaginary frequency at the optimized transition state (**TsA2**, Figure 2) does describe the carbonyl oxygen nucleophilic attack onto the carbon vicinal to the protonated ether (C_2, see Scheme 4) and the release of methanol as the leaving group (for R = Me the forming bond is 2.01 Å and the breaking one is 1.94 Å, while for R = *t*Bu, we find 2.01 and 1.92 Å). Very remarkably, the barriers calculated for this path (22.2 and 18.6 kcal mol^{-1} for **1a** and **1d**, respectively) are in very good agreement with the experimental ones (25.8 ± 1.5 (**1a**) and 22.4 ± 0.7 (**1d**)). Moreover, the cyclic intermediate **IntA2** is lower in energy than the reactant **ProtA1**; that is, the process is exergonic (1.4 and 4.3 kcal mol^{-1} for Me and *t*Bu, respectively).

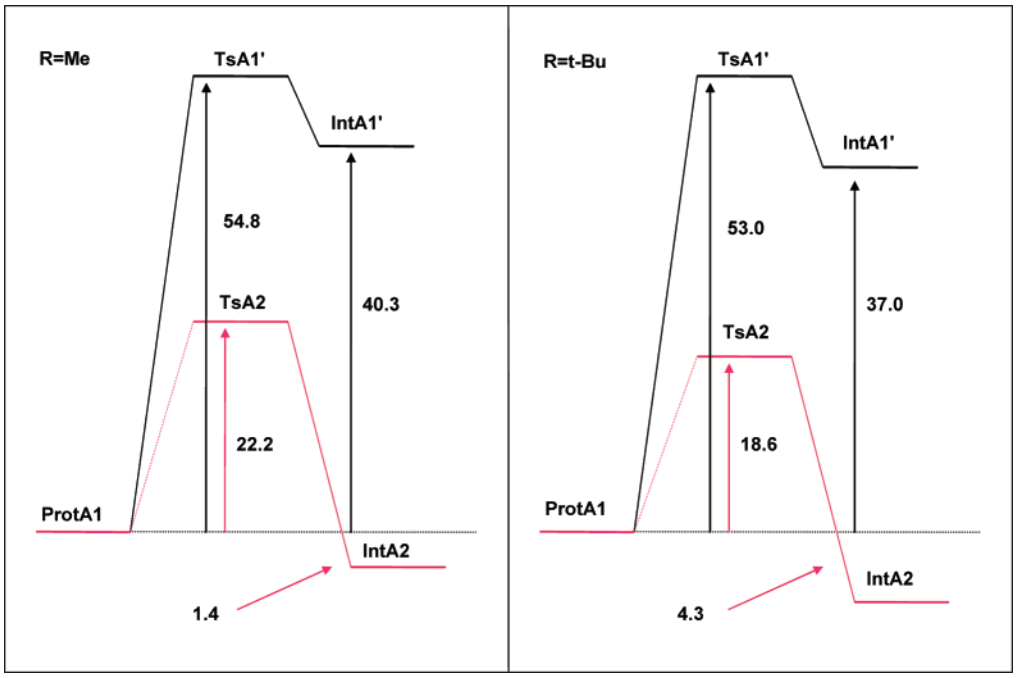

FIGURE 1. Free energy profiles (kcal mol^{-1}) for the **A1′** and **A2** mechanisms. Free energy barriers are calculated for both paths as the energy difference between the lowest and the highest critical points located on the PES in the course of the reaction from **Rx** to **IntA1′** or **IntA2**. Note that the starting point for both mechanisms (which the barrier refers to) is always **ProtA1**, that is, the more stable protomer found at the acidic experimental conditions. Moreover, for the **A2** mechanism, only the overall free energy variation between **ProtA1** and **TsA2**, which are species not directly connected (discontinuous line), is reported.

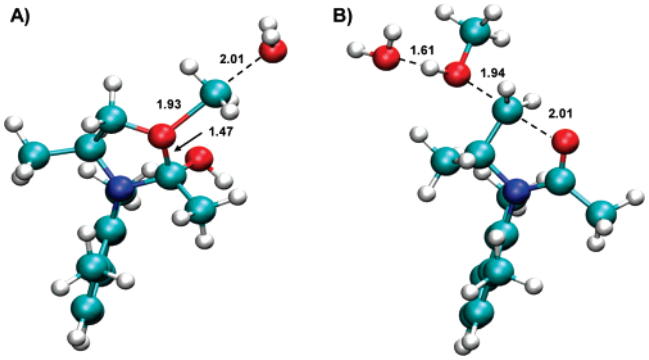

FIGURE 2. Optimized structures of the transition states **TsA1′** (A) and **TsA2** (B) for **1a** (R = Me).

SCHEME 4

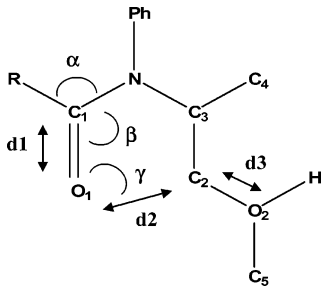

In conclusion, although carbonyl protonation is more favored compared to that involving the ethereal oxygen, it leads to a blind alley with unsurpassing barriers for the formation of the oxonium intermediate. On the other hand, the formation of the less stable protonated form appears as a compulsory step in the anchimeric assistance process. In fact, it opens the way to a favored low-energy path with barriers in agreement with the experimental results. Basicity of the carbonyl amide oxygen is a drawback in the initial protonation, but its nucleophilicity is an advantage at the end of the first step, and the last overrides the initial disadvantage. Thus, we can reasonably assert that the anchimeric assistance of the vicinal amide group is carried out through the **A2** mechanism. This reaction is intramolecularly assisted because the methanol departure from previously protonated ethereal oxygen is facilitated by formation of the new O−C bond that derives from the attack of the carbonyl amide.

(c) 1a (R = Me) versus 1d (R = *t*Bu): A Comparison. In light of the results presented above, it is apparent that the reaction proceeds via the **A2** route. Now, we need to rationalize the difference in the reaction rates observed for the two different substituents. The **A2** profiles discussed in this section have been recomputed without any explicit water (see the discussion below), and also the less stable protomers **ProtA2** and its rotamers **NAC**[7,8] (near attack conformation) have been included in this analysis (Figure 3; see Tables S1 and S2 in the Supporting Information for the geometrical parameters and atomic point charges of the stationary points involved in the reaction). The energy gap between **ProtA1** and **TsA2** is 3.6 kcal mol^{-1} higher than the one computed with the explicit water molecule (compare the energy profiles in Figures 1 and 3); the reason is that this water better stabilizes the methanol leaving group in **TsA2** by hydrogen bonding (see Figure 2) than the dielectric continuum model alone does (it is known that these models fail to include short-range effects as hydrogen bond). In **ProtA1**, the hydrogen bond is intramolecular, so the explicit water has only a weak effect on the energy of this critical point. Thus, by eliminating the explicit water molecule, we observe an increase in the activation barrier due to the loss of the explicit hydrogen bond in **TsA2**. Anyway, we decided to eliminate this water because it can affect computational accuracy by generating conformational problems (see the **NAC** analysis below). In fact,

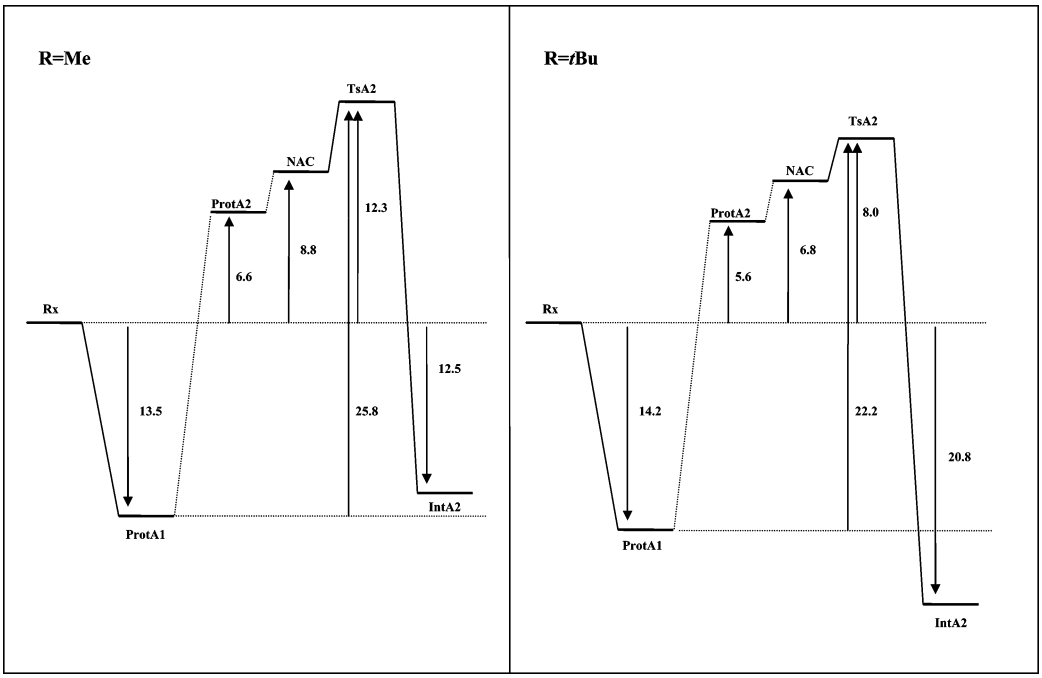

FIGURE 3. Free energy profiles (kcal mol^{-1}) for the reactions following the **A2** mechanism, computed without an explicit water molecule. **ProtA1** and **ProtA2**, **ProtA2** and **NAC** are linked by discontinuous lines because they are not directly connected; the corresponding transition states have not been calculated because these processes occur fast and are determined by equilibrium constants.

the water molecule can interact with the substrate in a lot of different ways, producing a plethora of stable minima and transition states.

Since intramolecular cyclization represents the bottleneck for this route, a rationale for the different reaction rates observed for the two substituents may be attempted by applying the conformational **NAC** theory that has been introduced by Bruice and co-workers[7,8] for similar problems. The term **NAC** defines the required conformation for juxtaposed reactants that geometrically must be formed prior to reaching a transition state in a reaction pathway. Lighstone and Bruice[7,8] have underlined the importance of "*active*" ground-state conformations of the substrate on the reaction rates: the greater the mole fraction of reactant conformations that are present as **NACs**, the greater the rate constant. Inspired by this kinetic reactivity model, we pursued a systematic conformational search (hence the need to remove the explicit water molecule, as explained above), followed by QM optimizations, for identifying the most stable **NAC** structures for R = Me (**1a**) and R = *t*Bu (**1d**) (see Figure 4).

These structures are located as fully unconstrained local minima (i.e., these are conformers) on the PES with O_1-C_2 distances of 2.65 Å (**1a**) and 2.59 Å (**1d**). The $O_1-C_2-O_2$ angles of approach is 167.1° (**1a**) and 167.6° (**1d**), well within the ideal cone of 30° with respect to the perfect angle of attack (180°) of a nucleophile in a S_N2 process.

The major difference between the two **NAC** structures is due to the *pushing effect* of the *t*Bu; Figure 5a displays the superposition of the **NAC** structures for **1a** and **1d**: we can clearly see this pushing effect if we analyze the difference in the α angle (118.1 and 123.8° for **1a** and **1d**, respectively). This is caused by the steric hindrance of the *t*Bu group that pushes the amidic carbonyl closer to the C_2 atom (i.e., $d2$ = 2.589 Å in **1d**, while it is 2.654 Å in **1a**), allowing for a better interaction between the lone pair of the amide carbonyl with the electrophilic C_2 carbon. This makes the **NAC** derived by the *t*Bu substituent energetically more favorable (i.e., more stable) than with Me. These **NAC** structures can be seen as being derived from **ProtA2**, in which the ethereal oxygen is protonated, with the $N-C_3-C_2-O_2$ dihedral angle that goes from 48.2 to 125.0° (Figure 5b shows the rotation of the dihedral angle from **ProtA2** to the **NAC** for **1a**): energetically, this rotation costs only 2.2 (**1a**) and 1.2 kcal mol^{-1} (**1d**), and this provides a nice rationale for their energies (see Figure 3). Using the Boltzmann distribution, we can calculate the probability of formation of the **NAC** structures for the two substrates, starting from the more stable species **ProtA1**. Because there is an energy difference of 1.3 kcal mol^{-1} between the two **NAC** conformations (**NACs** are 22.3 (R = Me) and 21.0 kcal mol^{-1} (R = *t*Bu) higher than **ProtA1**), we predict a **NAC** population for the *t*Bu substituent that is about 7.6 times bigger than that for Me.[44] It is apparent that this is one of the most important contributions responsible for the greater reaction rate observed for the *t*Bu substituent as compared to the Me one.

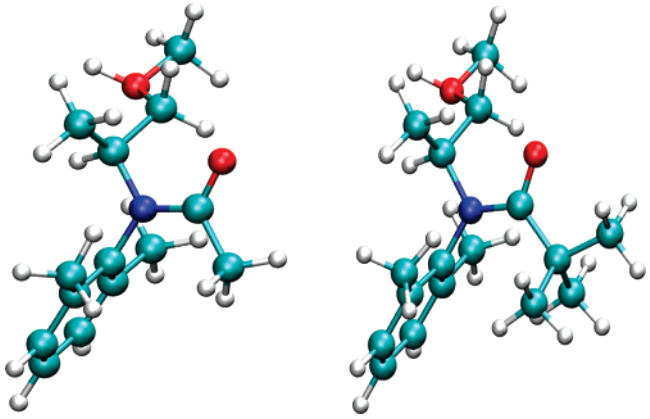

FIGURE 4. Optimized structures of the **NAC** for **1a** (R = Me) and **1d** (R = *t*Bu).

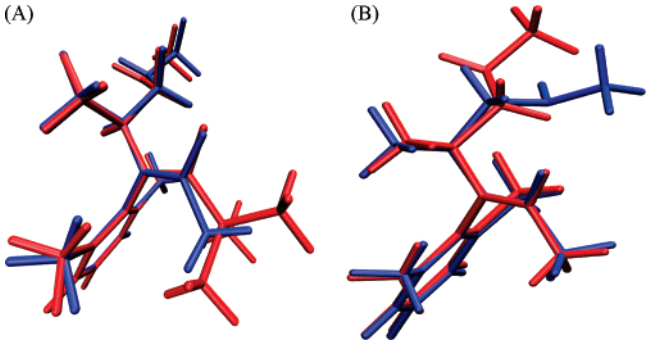

FIGURE 5. (A) Superposition of **NAC** structures for **1a** (R = Me, blue) and **1d** (R = *t*Bu, red). (B) Superposition of **ProtA2** (blue) and the **NAC** (red) structure for **1a** (R = Me).

The statistic analysis of **NAC** population given above already provides a qualitative rationale for the greater reaction rate observed for **1d**. Anyway, it is apparent that the energetics computed along the **A2** reaction profile can also be used to provide an additional (and more quantitative) explanation for the higher rate observed using a *t*Bu substituent instead of a Me. Inspection of the calculated free energy (*G*) profiles (see Figure 3) reveals that the activation barrier is 25.8 kcal mol^{-1} for R = Me, while it is 22.2 kcal mol^{-1} for R = *t*Bu. Very remarkably, these values are in striking good agreement with the previously reported[23] experimental values of 25.8 ± 1.5 (**1a**) and 22.4 ± 0.7 (**1d**) kcal mol^{-1} (see Table 1).

The experimental difference between the two activation barriers is 3.4 kcal mol^{-1}, which is very close to the computed one (3.6 kcal mol^{-1}). We have just shown above (by the **NAC** approach) that a contribution of 1.3 kcal mol^{-1} to this energy difference is due to the pushing effect that favors the *t*Bu substituent. Thus, we still need to explain the origin of the residual energy difference in the activation barriers, in order to have a quantitative explanation of the substituent effects. For this reason, we have to investigate the difference between the barriers that lead from the **NAC** structures to the transition state. It turns out that a geometrical analysis alone cannot provide an explanation for the computed (and observed) energetic differences since the molecular structures and the geometrical parameters defining the reactive modes along the reaction coordinate are very similar for both the substituents along the cyclization path; for example, *d*2 (which defines the approaching distance of the nucleophile) is the same (2.11 Å) and *d*3 is 1.86 (R = Me) and 1.83 Å (R = *t*Bu) at **TsA2**, while *d*2 is 1.48 (R = Me) and 1.47 Å (R = *t*Bu) and *d*3 is 2.99 (R = Me) and 3.23 Å (R = *t*Bu) at **IntA2**.

On the other hand, an electrostatic analysis (see Table S2 in the Supporting Information for values of the charges) turns out to be a helpful tool to explain the residual energy difference. While charges at O_1 and C_2 atoms are those that are mostly changing through the course of the reaction because these centers are directly involved in the reactive process, they cannot give useful information about the different rates observed for **1a** and **1d**, as their behavior is the same in the two systems. Specifically, we have to take into account the electronic effects of the R substituent along the path from **NAC** to the transition state **TsA2**. While a significant positive charge always appears at the C_1 carbon all along the path, it is apparent that the R group stabilizes (via positive charge delocalization) **TsA2** better than **NAC**: note (see Table S2 in the Supporting Information) that a higher positive charge is delocalized on R at the transition state (−0.004 and 0.192 for Me and *t*Bu substituent, respectively) than at the **NAC** (−0.043 and 0.125 for Me and *t*Bu substituent, respectively). Thus, *t*Bu leads to a lower activation barrier than Me since it is a better electron-donating group, and the overall stabilization effect on the activation barrier is greater (note that going from **NAC** to **TsA2** costs 1.2 and 3.5 kcal mol^{-1} for *t*Bu and Me, respectively). The same reasoning accounts for the 6.2 kcal mol^{-1} exergonic (1.0 kcal mol^{-1} endergonic) cyclization process computed for **1d** (**1a**). This can also be addressed by the different ability of the R groups in delocalizing (i.e., stabilizing) the positive carbocationic charge: it is apparent that *t*Bu stabilizes the cyclic cationic product better than Me, thus leading to an exergonic process.

An alternative way to look at these effects refers to the different nucleophilicity of the reactant: it is apparent that *t*Bu (being a better electron-donating group than Me) leads to a stronger nucleophile, thus accelerating the process.

(d) Comparison between the A2 Mechanism and the Catalytic Mechanism in β-Hexosaminidases and O-GlcNAcases Enzymes. β-Hexosaminidases and O-GlcNAcases are very important enzymes involved in multiple cellular processes. They catalyze the hydrolytic cleavage of β-O-linked GlcNAc (2-acetamido-2-deoxy-D-glucopyranose) from post-translationally modified serine and threonine residues of nucleocytoplasmic proteins, and a large number of diseases have been associated with their disregulation, including diabetes, Alzheimer's disease, and cancer.

The proposed catalytic mechanism in the glycosidic bond breaking step is displayed in Figure 6.

Although the details of the process are not yet completely clear, it involves a nucleophilic attack of the 2-acetamido group of the substrate on the anomeric carbon. It is apparent that an anchimeric assistance of the acetamido group occurs in this reaction, as well, which is very similar to the one investigated here. In fact, following the commonly accepted mechanism, the first step of the reaction is the nucleophilic attack of the 2-acetamido carbonyl oxygen on the anomeric carbon to form a covalent bicyclic oxazoline intermediate. This step is facilitated by the polarization of the 2-acetamido moiety by Asp174, acting as a general base catalyst. Departure of the leaving group is then facilitated by general acid catalysis provided by another carboxyl group in the enzyme active site, Asp175. In the second step, an activated water molecule attacks the anomeric center and the oxazoline intermediate is opened, leading to the final glycosidic bond breaking product.

Important analogies appear if we compare this mechanism with the **A2** route investigated in this paper: (1) An oxazoline intermediate is formed that derives from the nucleophilic attack of the carbonyl amide. (2) A mechanism of general acid catalysis is involved that facilitates the departure of the leaving group (it triggers the cyclization reaction in our system). (3) The reaction rate is proportional to the nucleophilicity of the carbonyl amide. We have demonstrated here that the higher the electron-donating ability of the *N*-acetyl substituent, the faster the reaction rate of the process: *t*Bu leads to a 100-fold reaction rate increase compared to the methyl substituent. Interestingly, Macauley and co-workers[14] synthesized several substrate analogues bearing differing levels of fluorine substitutions on the *N*-acetyl group. They demonstrated that the highly electronegative fluorine substituents (that decrease the nucleophilicity of the carbonyl group) have a deleterious effect on the catalysis, slowing down

(44) The calculation is simply based on the Boltzmann distribution NAC-(*t*Bu)/NAC(Me) = $e^{-\Delta E/KT}$.

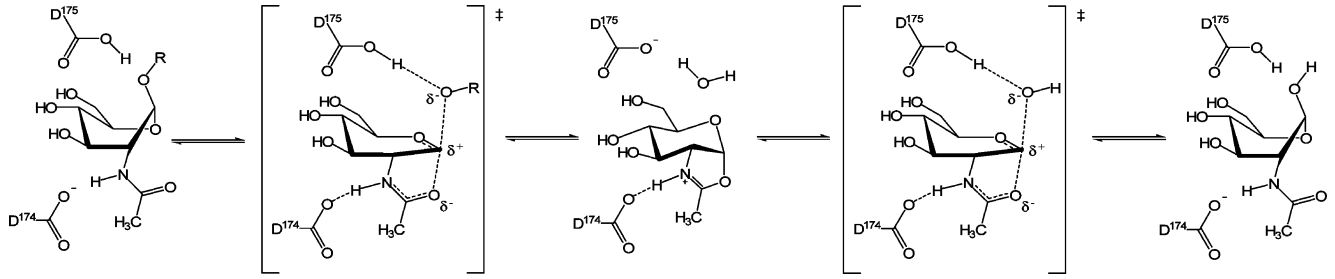

FIGURE 6. Catalytic mechanism of O-GlcNAcase enzyme involving substrate-assisted catalysis.

dramatically the reaction rate, in agreement with our computationally based analysis.

In conclusion, the system studied in this work can be considered a useful biomimetic model for the catalyzed (anchimerically assisted) glycosidic bond cleavage in β-hexosaminidases and O-GlcNAcases enzymes, which can be used as a reference model for further computational/experimental studies.

Conclusions

In this paper, we describe a realistic model for the anchimerically assisted acid-induced ether cleavage. On the basis of experimental results,[17−23] two mechanisms were previously suggested that have been investigated here: the first (**A1** mechanism) involves a nucleophile ethereal oxygen that attacks the protonated amide group, and the second (**A2** mechanism) involves the nucleophilic attack of the amide group on C_2, the carbon adjacent to the protonated ethereal oxygen. We unambiguously demonstrated that the anchimeric assistance of the amide group is carried out through the **A2** mechanism. Although carbonyl protonation is much more favored compared to that involving the ethereal oxygen, the attack of the ether on the protonated amide group is too high in energy to be competitive. On the other hand, the free energy profile calculated for the **A2** mechanism is in good agreement with the standard free energy of activation[23] recorded experimentally for both **1a** and **1d**. Most remarkably, we have also provided a rationale for the kinetic results, specifically the more than 100-fold higher reaction rate observed for the *t*Bu substituent (**1d**) compared to that of Me (**1a**). Two concurrent reasons have been called to account for this behavior: (1) a **NAC** population for the *t*Bu substituent that is about 7.6 times bigger than that for Me; (2) a grater effect of *t*Bu in stabilizing the transition state (or in increasing the nucleophilicity of the reactant) for the **A2** process, which is due to its better electron-donating effect.

Interestingly, the discussed mechanism of anchimeric assistance by the vicinal amide group has many analogies with the one used in the enzymatic activity of important glycosidases, such as β-hexosaminidases and O-GlcNAcases. In fact, these enzymes are known to use substrate-assisted catalysis, where the 2-acetamido group of the substrate directly participates in the reaction, thus anchimerically assisting this process. In conclusion, the system studied in this work can be viewed as a general biomimetic model for the catalyzed glycosidic activity of β-hexosaminidases and O-GlcNAcases.

Acknowledgment. The authors thank Professor Gianni Porzi for many useful discussions regarding his experimental work on this system. We would like to thank M.U.R.S.T. (Cofin 2005, Progetto Nazionale "Sintesi e Stereocontrollo di Molecole Organiche per lo Sviluppo di Metodologie Innovative di Interesse Applicativo") and Bologna University (Progetti Strategici d'Ateneo 2005: Progetto CompRenDe) for the financial support of this research. M.G. is also grateful for a FIRB (RBAU01L2HT). We wish to thank CINECA and INSTM for granted calculation time.

Supporting Information Available: Detailed discussion on protonation equilibria, optimized structures and energies of the protomers discussed in the text (Figure S1), geometrical parameters and atomic point charges (Tables S1 and S2) of the stationary points involved in the reaction, the coordinates of all the B3LYP/6-31G*optimized critical points discussed in the text, their absolute energies, and number of imaginary frequencies. This material is available free of charge via the Internet at the http://pubs.acs.org.

JO701394Z